metals

MDPI

Article

Deformation Behavior and Microstructure Evolution of High-Strength and -Toughness Ti55531 Titanium Alloy

Yucheng Yang [1], Tongsheng Deng [1,2,3,*], Zhi Liu [1], Hai Liu [1], Yupeng Yuan [1] and Wei Chen [1]

[1] School of Materials Science and Engineering, Jiangxi University of Science and Technology, Ganzhou 341000, China; 6120220220@mail.jxust.edu.cn (Y.Y.); l2317447603@163.com (Z.L.); lh19859722917@163.com (H.L.); 15128636630@163.com (Y.Y.); 1320230344@mail.jxust.edu.cn (W.C.)
[2] Jiangxi Provincial Key Laboratory of High-Performance Steel and Iron Alloy Materials, Ganzhou 341000, China
[3] Jiangxi Provincial Key Laboratory of Power Batteries & Energy Storage Materials, Ganzhou 341000, China
* Correspondence: dts115@jxust.edu.cn

Abstract: In this paper, constant strain rate compression was carried out by means of an MMS-100 thermal/force simulation tester in a temperature range of 790~940 °C, with a strain rate of 0.01–1 s^{-1} and a compression volume of 60%. A linear regression method was used to fit the relationship between strain stress, strain rate, and deformation temperature, and the Arrhenius-type constitutive equation of Ti55531 titanium alloy was established; the heat deformation activation energy of Ti55531 titanium alloy was obtained as 211,747.5 kJ·mol^{-1}. A thermal processing map of Ti55531 alloy was established. EBSD results show that after hot compression, the recrystallization volume fraction greatly increased. The original sample recrystallization volume fraction was 23.2%. Under a deformation temperature of 850 degrees Celsius and deformation rate of 0.01, the recrystallization volume fraction rose to 38.5%; after the annealing process, the recrystallization volume fraction further increased to 72.6%. Under the deformation temperature of the thermal compression process, the higher the deformation rate, the larger its recrystallization volume fraction. After annealing, the recrystallization volume fraction further increased. This study can provide a reference and theoretical guidance for the development and optimization of the thermal processing process of Ti55531 titanium alloy.

Keywords: Ti55531 titanium alloy; deformation behaviors; microstructural evolution; constitutive model; thermal processing diagram

check for updates

Academic Editor: Marcello Cabibbo

Received: 30 December 2024
Revised: 25 January 2025
Accepted: 30 January 2025
Published: 10 February 2025

Citation: Yang, Y.; Deng, T.; Liu, Z.; Liu, H.; Yuan, Y.; Chen, W. Deformation Behavior and Microstructure Evolution of High-Strength and -Toughness Ti55531 Titanium Alloy. *Metals* **2025**, *15*, 176. https://doi.org/10.3390/met15020176

Copyright: © 2025 by the authors. Licensee MDPI, Basel, Switzerland. This article is an open access article distributed under the terms and conditions of the Creative Commons Attribution (CC BY) license (https://creativecommons.org/licenses/by/4.0/).

1. Introduction

Titanium and its alloys have been widely used in the aerospace and marine fields due to their high strength-to-weight ratios, excellent fracture toughness, and good corrosion/oxidation resistance [1]. Near-β titanium alloys contain high weight percentages of stabilized beta-phase elements, such as vanadium (V), molybdenum (Mo), and chromium (Cr); these alloys can retain a full β phase even after quenching and have a low β transus temperature (Tβ), a wide processing window, high hardenability, and high strength [2]. Due to these properties, they have become the alloys of choice for large aerospace parts, such as landing gear forgings, nacelles, fuselages, and wings [3]. These parts usually play important roles in aerospace equipment; consequently, they require better mechanical properties. Therefore, thermomechanical processing is usually adopted not only for shaping but also for controlling the microstructure and adjusting their mechanical properties. However, near-β titanium alloys are very sensitive to the processing parameters. During a deformation process, the microstructure may be subjected to complex evolutions, such as grain

growth or coarsening, dynamic recrystallization (DRX) in the β phase, dynamic recovery, phase transformation, and precipitation. All of these evolutions can change the grain size, morphology, and phase volume fraction and also influence the mechanical properties. Therefore, a deep understanding of the microstructural evolution during deformation is essential for optimizing the thermomechanical processing and controlling the microstructural evolution [4]. Many studies have reported the microstructural evolution and flow softening during the isothermal deformation of near-β titanium alloys. Shi et al. [5] found that the dynamic recrystallization (DRX) behavior of Ti-55511 alloy showed significant differences under different deformation conditions. Discontinuous dynamic recrystallization tends to be the dominant mechanism at low temperatures, and as the temperature increases, the continuous dynamic recrystallization mechanism gradually dominates. Matsumoto et al. [6] similarly pointed out that the main softening mechanisms of Ti-5553 titanium alloy above 800 °C are dynamic recovery and continuous dynamic recrystallization. Li et al. [7] systematically investigated the texture evolution of Ti-6554 alloy and further analyzed its effect on dynamic softening. The texture evolution was accompanied by dynamic phase transition and dynamic spheroidization. This led to a complex evolution of the α phase texture during the deformation process. Lu et al. [8] studied the dynamic softening phenomenon from the thermodynamic and microstructural evolution perspective and calculated the quantitative relationship between texture evolution and flow softening by Schmidt factors of Ti-35421 alloy. They found that with increasing deformation, the grains gradually evolved to soft orientation and thus caused flow softening. Recently, many researchers have begun to investigate the deformation behavior and microstructural evolution (such as DRV [9], DRX, and the softening mechanism [10]) of a new high-strength titanium alloy, Ti-5Al-5Mo-5V-3Cr-1Zr (Ti55531). In addition, the present experimental results indicate that the DPT occurs noticeably in the Ti55531 alloy isothermally deformed in the α+β region. Moreover, the DPT has a significant effect on the flow softening of Ti55531 alloy. Thus, it is essential to disclose the flow behavior and microstructural evolution of Ti55531 alloy to provide some guidelines for processing design and microstructure tailoring. However, few studies systematically report the flow behavior, texture evolution, and DPT of Ti55531 alloy during hot deformation.

In the present study, hot compressive tests were carried out to research the flow behavior of Ti55531 alloy. The morphological evolution of Ti-5Al-5Mo-5V-3Cr-1Zr (Ti55531) material was analyzed using optical microscopy (OM) and electron backscatter diffraction (EBSD) techniques, as well as the recrystallization volume fraction. The effects of different temperatures, rates, and annealing processes on the high-temperature deformation were analyzed. In the study, after the isothermal compression test, the compressed samples under different conditions were recrystallized and annealed; the changes in dynamic recrystallisation volume fraction are shown in detail by EBSD, which provides a basis for the microstructure changes.

2. Materials and Experimental Procedure

A near-β titanium alloy (Ti55531) was used in this study. The measured chemical compositions (wt%) were 5.0% aluminum (Al), 5.0% molybdenum (Mo), 5.1% vanadium (V), 3.0% chromium (Cr), 1.0% zirconium (Zr), 0.08% iron (Fe), and 0.1% other elements; Ti made up the remainder. The Mo, V, Cr, and Fe stabilize the β phase, whereas the Al and other elements stabilize the α phase. The corresponding α transformed into β transus temperature (Tβ) was 845 °C [11]. The cylindrical specimens were 15 mm high and 10 mm in diameter and were electro-discharged from the received machined material (forged billet) [12].

The isothermal compression experiments were performed at temperatures of 790 °C–940 °C and at strain rates from 0.01 s^{-1} to 1 s^{-1} on an MMS-100 simulator (Shenyang Keanjie Material Technology Co., Ltd., Shenyang, China). Prior to the de-

formation, each specimen was heated to the tested temperature for 5 min to ensure a uniform temperature distribution throughout the specimen. The deformation temperature was measured by a thermocouple that was spotwelded to the center of the specimen's surface. To reduce the die friction and ensure uniform deformation, two thin pieces of thallium were affixed to the flat dies. To preserve the microstructure at high temperatures, the compressed samples were water-quenched immediately after the compression tests. The deformation procedure is shown in Figure 1.

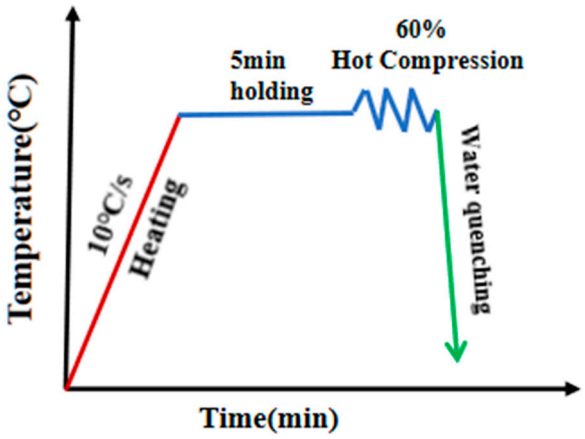


Figure 1. Isothermal compression schematic.

Following the hot compression experiments, metallography was used to analyze the microstructural evolution. The deformed specimens were cut along their long axis, mechanically ground using grit papers with different particle sizes, and polished and etched with a solution of hydrofluoric acid (vol.20%), nitric acid (vol.10%), and water (vol.70%) for microstructural observations. Optical micrographs were then shot at 50× magnification in the central region of the specimens using a metallurgical microscope. The microscope used is shown in Figure 2; an RX50M metallurgical microscope (Huizhou Tianzhuo Chuangzhi Instrument Equipment Co., Ltd., Huizhou, China) was used. The hot compression samples (850 °C, 0.01), (850 °C, 1), and (850 °C, 1) were taken for recrystallization annealing treatment at a recrystallization annealing temperature of 750 °C and a holding time of 3 h, followed by air cooling. A comparison of the microstructural changes in the hot compression samples at different temperatures and rates before and after recrystallization annealing was carried out.



Figure 2. RX50M metallurgical microscope.

The hot-compressed specimen was cut in half in the direction of the heat compression using a wire-cut device (Suzhou Longkai Electromechanical Technology Co., Ltd., Suzhou, China), and one half of the specimen was frosted, polished, etched, and then observed using a scanning electron microscope (Ningbo Sainyu Instrument Co., Ltd., Ningbo, China).

The other half was electrolytically polished to make the EBSD specimen. EBSD examination was carried out via a ZEISS Sigma 500 field emission scanning electron microscope equipped with an Oxford Nordlys Max3 EBSD probe (Huacheng Intelligent Equipment, Suzhou, China). The step size was 0.3 μm and the acceleration voltage was 20 kV. EBSD data were processed and analyzed using channel 5 software (2019v5.12) [13].

3. Experimental Results and Discussion

3.1. True Stress–Strain Curves

Figure 3 shows the true stress–true strain curves of Ti55531 titanium alloy during isothermal compression under different deformation conditions. It can be seen that the rheological stress decreases with the increase in deformation temperature and increases with the increase in strain rate, which indicates that the deformation temperature and strain rate have a significant effect on the rheological stress. In the early stage of deformation, the rheological stress is affected by work hardening and increases rapidly with the increase in strain rate, and when the rheological stress reaches the peak, it starts to decrease gradually due to the softening effect [14]. This is because at the early stage of deformation, the number of dislocations inside the material increases with the increase in deformation, and the resistance to dislocation movement also increases, so that work hardening dominates. When the amount of strain is large enough, a large number of dislocations undergo climb and cross-slip shifts, and at the same time, the energy stored in the material during deformation activates the onset of dynamic recrystallization, which acts as a softening agent, so that the rheological stress gradually decreases after the peak stress. In addition, it can be seen from Figure 3 that the higher the deformation temperature, the lower the degree of work hardening and the earlier the flow softening phenomenon occurs. This is because dynamic recrystallisation is a thermally activated behavior, and higher deformation temperatures and rates make the atoms in the material more energetic and reactive, and thus more prone to atomic diffusion and vacancy diffusion, reducing the cross-slip and creep resistance of dislocations and thus making dynamic recovery and dynamic recrystallisation more likely to occur [15]. At higher deformation temperatures, the degree of work hardening of the material is lower and can enter the flow softening stage earlier [16].

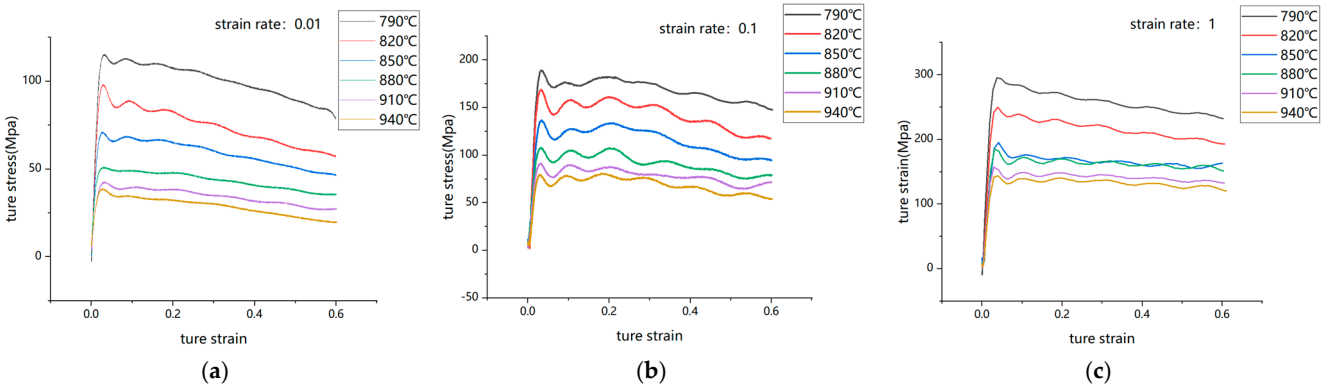


Figure 3. True stress–true strain curves under different deformation conditions. (**a**) 0.01 s^{-1}; (**b**) 0.1 s^{-1}; (**c**) 1 s^{-1}.

3.2. High-Temperature Deformation Equation

For a given metallic material, the rheological stress is only related to the deformation temperature, strain rate, and strain; therefore. in this paper, the widely used Arrhenius equation proposed by SELLARS C M and MCTEGART W J [17] is used to describe the relationship between the rheological stress and the strain rate and the deformation temperature:

$$\varepsilon = f(\sigma)exp\left(\frac{Q_1}{RT}\right) \tag{1}$$

In (1), $f(\sigma)$ takes the following three forms:

$$\begin{array}{ll} f(\sigma) = A_1\sigma^{n_1} & \text{(low stress levels);} \\ f(\sigma) = A_3exp(\beta\sigma) & \text{(high stress levels);} \\ f(\sigma) = A_3[sinh(\alpha\sigma)]^n & \text{(all stress levels).} \end{array} \tag{2}$$

In the above equation, ε is the strain rate; σ is the rheological stress (MPa); Q_1 is the thermal deformation activation energy (J·mol^{-1}); R is the gas constant, with R = 8.314 J·mol^{-1}; T is the absolute temperature (K); and A_1, A_2, A_3, n, n_1, α and β are material constants, with $\alpha = \beta/n_1$. Since the hyperbolic sine function in Equation (2) is applicable to both low and high stress levels, this paper chooses the hyperbolic sine function to establish the constitutive equation of Ti55531 titanium alloy [18].

Substituting the power and exponential functions in Equation (2) into Equation (1) and taking logarithms of their ends gives the following:

$$ln\varepsilon = n_1 ln\sigma + lnA_1 - \frac{Q_1}{RT} \tag{3}$$

$$ln\varepsilon = \beta\sigma + lnA_2 - \frac{Q_1}{RT} \tag{4}$$

Substituting the experimental data in Figure 1 into Equations (3) and (4), the plots of lnε-lnσ and lnε-σ relations were made, respectively, as shown in Figure 4 The slopes of each straight line were obtained by linear regression and then averaged to obtain n_1 = 3.33 and β = 0.038, thus yielding α = 0.0114.

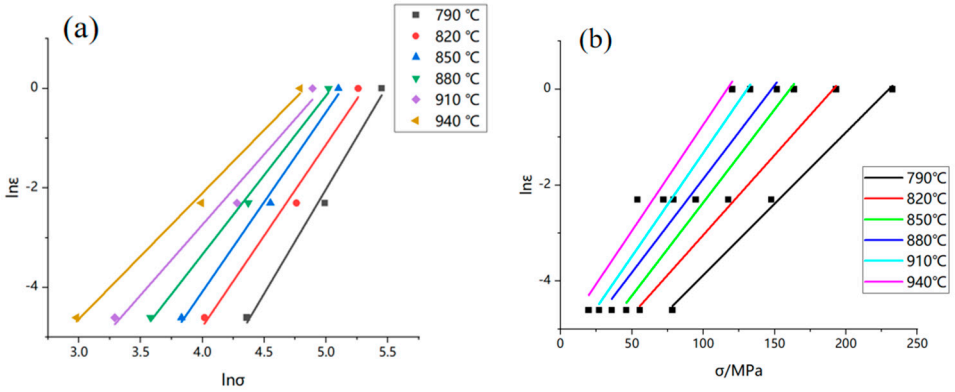


Figure 4. Ti55531 titanium alloy material constant relationship. (**a**) lnε-lnσ, (**b**) lnε-σ.

Substituting the hyperbolic sine function in Equation (2) into (1) and taking logarithms of its ends yields the following:

$$ln\varepsilon = nln\sigma[sinh(\alpha\sigma)] - \frac{Q_1}{RT} + lnA_3 \tag{5}$$

The compression experimental data of Ti55531 titanium alloy were substituted into Equation (5) and plotted as lnε-ln[sinh(ασ)] and ln[sinh(ασ)]-10,000/T, respectively, as shown in Figure 5. The slopes of the straight lines were obtained by linear regression, and then the average value was taken to obtain n = 2.8735, Q_1/Rn = 8863.333, and Q_1 = 211,747.498 J·mol^{-1}.

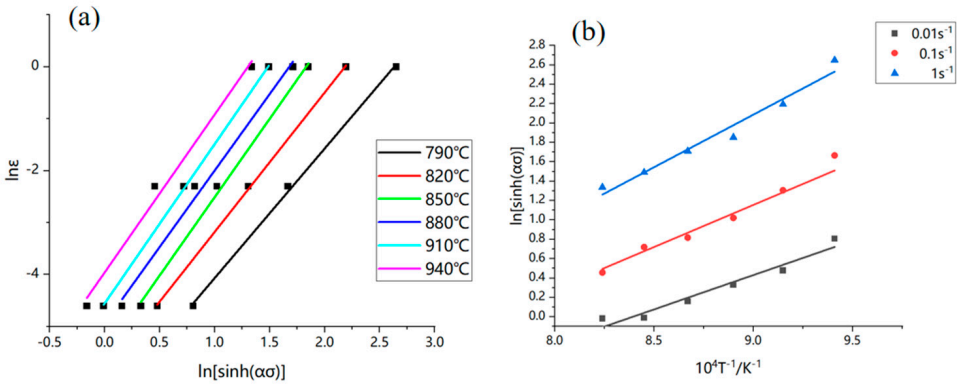


Figure 5. Relations of material constants of Ti55531 titanium alloy: (**a**) lnε-ln[sinh(ασ)]; (**b**) ln[sinh(ασ)]-10,000/T.

The effect of deformation temperature and strain rate on thermal deformation can be expressed in terms of Z-parameters as follows:

$$Z = \varepsilon exp\left(\frac{Q_1}{RT}\right) = A_3[sinh(\alpha\sigma)]^n \quad (6)$$

Taking logarithms of Equation (6) yields the following:

$$lnZ = nln\sigma[sinh(\alpha\sigma)] + lnA_3 \quad (7)$$

The compression experimental data of Ti55531 titanium alloy were substituted into Equation (7) to make a plot of the lnZ-ln[sinh(ασ)] relationship, as shown in Figure 6. The intercept of the straight line was obtained by linear regression and calculated.

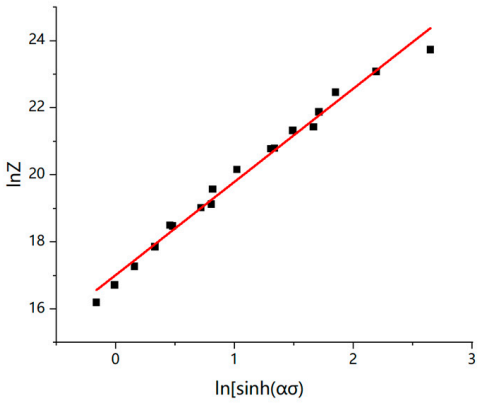


Figure 6. Relationship between lnZ-ln[sinh(ασ)].

The intrinsic equation of Ti55531 titanium alloy can be obtained according to the above requested parameters:

$$\varepsilon = 2.46 \times 10^7[sinh(0.0114\sigma)]^{2.8735}exp\left(\frac{-211747.5}{RT}\right)$$

3.3. Dissipation Diagram

In order to construct a thermal processing map of the alloy, Table 1 lists the data for the stress values corresponding to a true strain of 0.6 extracted from the true stress–true strain curve for the Ti55531 titanium alloy.

Table 1. Rheological stress values (σ/MPa) for Ti55531 titanium alloy at ε of 0.6.

Strain Rate (s^{-1})	790 °C	820 °C	850 °C	880 °C	910 °C	940 °C
0.01	80	55	46	36	27	19
0.1	147	117	94	79	72	54
1	232	193	163	151	134	120

When analyzing the stress–strain curves, mathematical methods are used in order to express the relationship more accurately, and in this experiment, a cubic polynomial fit was used to expand the data. Figure 7 shows the cubic spline curves of lnσ and lnε for Ti55531 titanium alloy with an ε of 0.6.

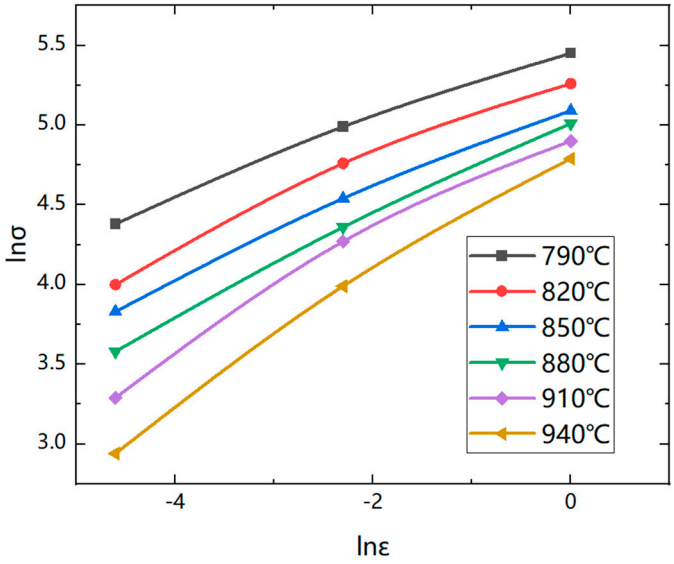


Figure 7. Cubic spline curves of lnσ and lnε for Ti55531 titanium alloy at strain of 0.6.

The slope lnσ/lnε of the points on the curve corresponding to the composition of different temperatures and different strain rates in Figure 8 is the value of the strain rate sensitivity index m of the alloy under different deformation conditions. The slope m value was obtained by using origin software to calculate the experimental data, as shown in Table 2.

Table 2. Values of strain rate sensitivity index m for Ti55531 titanium alloy.

Strain Rate (s^{-1})	790 °C	820 °C	850 °C	880 °C	910 °C	940 °C
0.01	0.2674	0.33	0.3083	0.3387	0.4255	0.4559
0.1	0.2323	0.2736	0.2736	0.3105	0.3496	0.4017

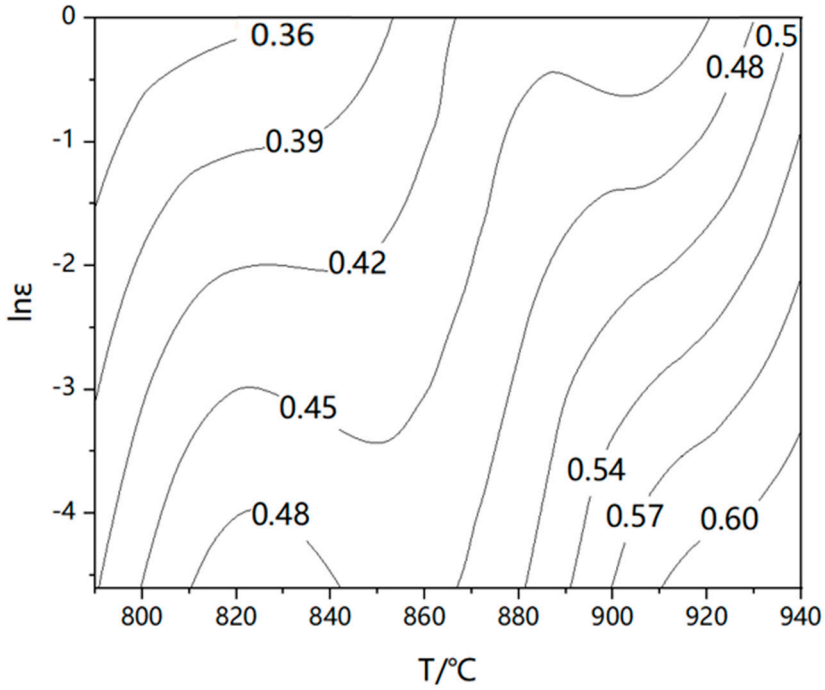


Figure 8. Power dissipation diagram of Ti55531 titanium alloy.

Table 3 shows the values of the power dissipation efficiency factor η for Ti55531 titanium alloy under different deformation conditions, respectively.

Table 3. Values of power dissipation efficiency factor η for Ti55531 titanium alloy.

Strain Rate (s^{-1})	790 °C	820 °C	850 °C	880 °C	910 °C	940 °C
0.01	0.4188	0.4962	0.4713	0.5060	0.5970	0.6263
0.1	0.3770	0.4296	0.4296	0.4739	0.5181	0.5732
1	0.3331	0.3569	0.3857	0.4404	0.4298	0.5158

The value of the power dissipation factor η for the alloy can be calculated from the equation $\eta = \frac{J}{J_{Max}} = \frac{2m}{m+1}$ combined with the data in Table 3.

3.4. Destabilization Diagram

In the actual forming and processing of titanium alloy, machining instability often leads to the occurrence of cracks, voids, and other defects [19].

According to the Prasad instability criterion, $\boldsymbol{\xi(\varepsilon) = \frac{\partial ln\left(\frac{m}{m+1}\right)}{\partial ln\varepsilon} + m < 0}$. It is known that there is a mathematical correlation between $ln\varepsilon$ and $ln\left(\frac{m}{m+1}\right)$. The mathematical correlation was calculated using cubic polynomials for the experimental data [20]. The cubic spline curves of Ti55531 titanium alloy at a strain of 0.6 for $ln\varepsilon$ and $ln\left(\frac{m}{m+1}\right)$ are shown in Figure 9. Based on this instability criterion, the values of the rheological instability criterion ξ for Ti55531 titanium alloy under different thermal processing conditions are shown in Table 4.

Figure 10 shows the instability diagram of Ti55531 titanium alloy at a strain of 0.6. The instability parameters of Ti55531 titanium alloy under the test conditions (temperature of 790–940 °C, deformation rate of 0.01–1 s^{-1}) are all positive. This indicates that all thermal processes occurred.

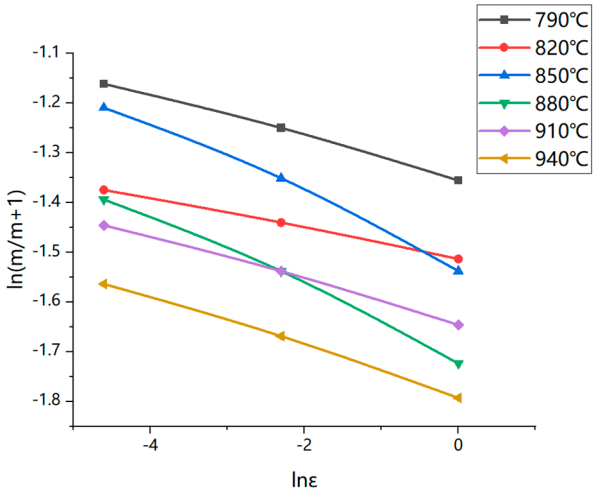


Figure 9. Cubic spline curves for Ti55531 titanium alloy for $ln\varepsilon$ and $ln\left(\frac{m}{m+1}\right)$.

Table 4. Rheological instability criterion values for Ti55531 titanium alloy.

Strain Rate (s^{-1})	790 °C	820 °C	850 °C	880 °C	910 °C	940 °C
0.01	0.2193	0.2675	0.2682	0.3102	0.3639	0.4174
0.1	0.1826	0.2020	0.2300	0.2803	0.2782	0.3595
1	0.1459	0.1365	0.1919	0.2506	0.1925	0.3017

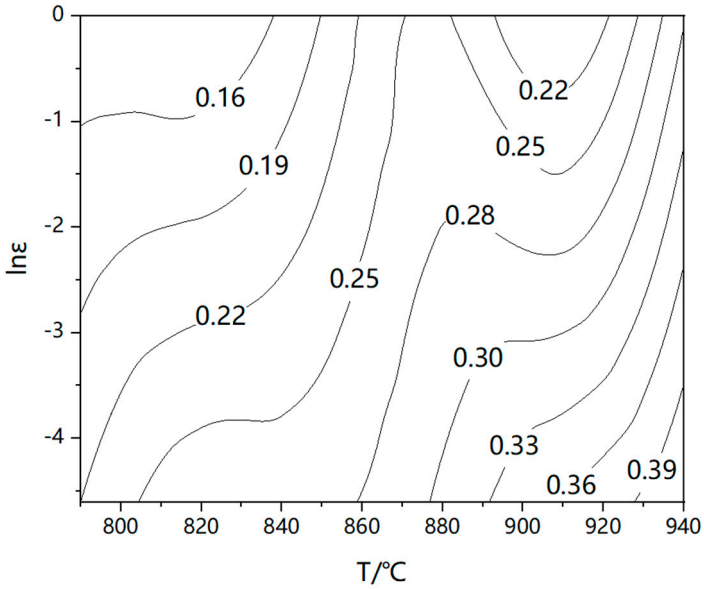


Figure 10. Instability diagram of Ti55531 titanium alloy.

3.5. Thermal Processing Diagram

The power dissipation map and the destabilization map of the material were superimposed to obtain the thermal processing map of the alloy. As shown in Figure 11.This was because of the fact that the alloy had no destabilization zone under this test condition (temperature of 790–940 °C; deformation rate of 0.01–1 s^{-1}).

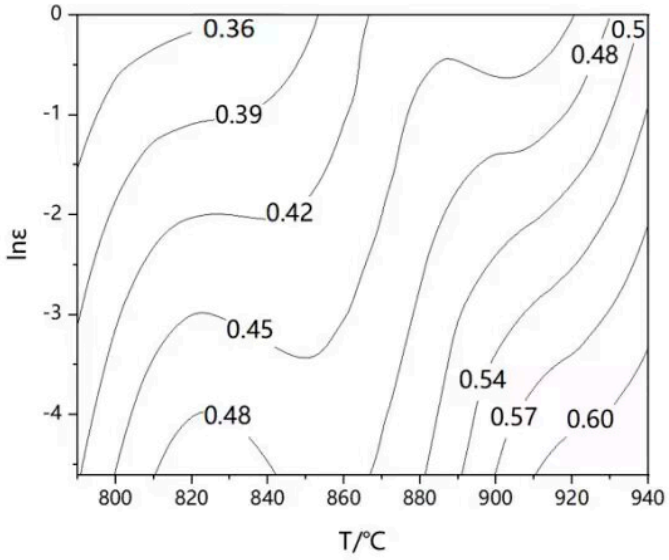


Figure 11. Ti55531 titanium alloy hot working diagram.

3.6. Microstructural Evolution

Figure 12 shows a metallographic under different experimental conditions after hot compression, where the graphs (a), (b), and (c) are the metallographic illustrations under the experimental conditions of (850 °C, 0.01 s^{-1}), (850 °C, 1 s^{-1}), and (910 °C, 1 s^{-1}) before recrystallization annealing, and the graphs (d), (e), and (f) are the metallographic illustrations after recrystallization annealing under the experimental conditions of (850 °C, 0.01 s^{-1}), (850 °C, 1 s^{-1}), and (910 °C, 1 s^{-1}) after recrystallization annealing. In (a), (b), and (c), according to the metallographic organization, equiaxial β grains can be seen. Some of the α phases are present near the grain boundaries. After annealing by recrystallization, it can be seen that new equiaxed grains are formed in the (d), (e), and (f) metallographic organization pictures, and the equiaxed grains are more uniform and finer, and the equiaxed α phase dissolves in the matrix.

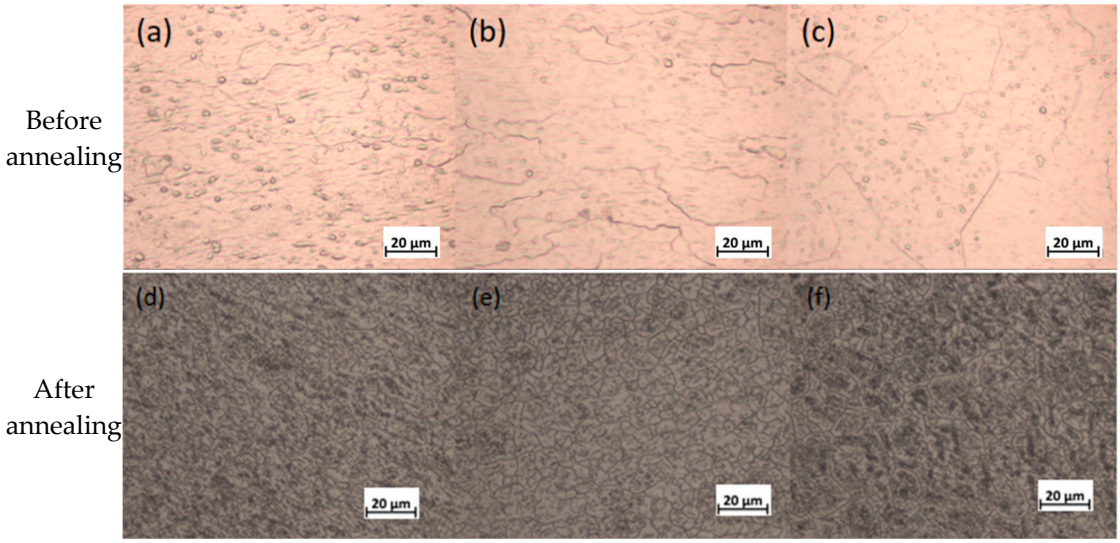


Figure 12. Photograph of metallographic organization of alloy after experiment: (**a**) 850 °C, 0.01 s^{-1}; (**b**) 850 °C, 1 s^{-1}; (**c**) 910 °C, 1 s^{-1}; (**d**) 850 °C, 0.01 s^{-1}; (**e**) 850 °C, 1 s^{-1}; (**f**) 910 °C, 1 s^{-1}.

Figure 13 shows SEM electron images under different experimental conditions after thermal compression, where panels (a), (b), and (c) are metallographic conditions before

recrystallisation annealing, (850 °C, 0.01 s^{-1}), (850 °C, 1 s^{-1}), and (910 °C, 1 s^{-1}), and (d), (e), and (f) are (850 °C, 0.01 s^{-1}), (850 °C, 1 s^{-1}), and (910 °C, 1 s^{-1}) before recrystallisation annealing. Prior to annealing, electron images of (a), (b), and (c) show that the equiaxed α phase is uniformly distributed on the β matrix, and that the equiaxed α phase is spherical in shape and has a long strip. After recrystallisation annealing, the equiaxed α phase is dissolved in the β matrix.

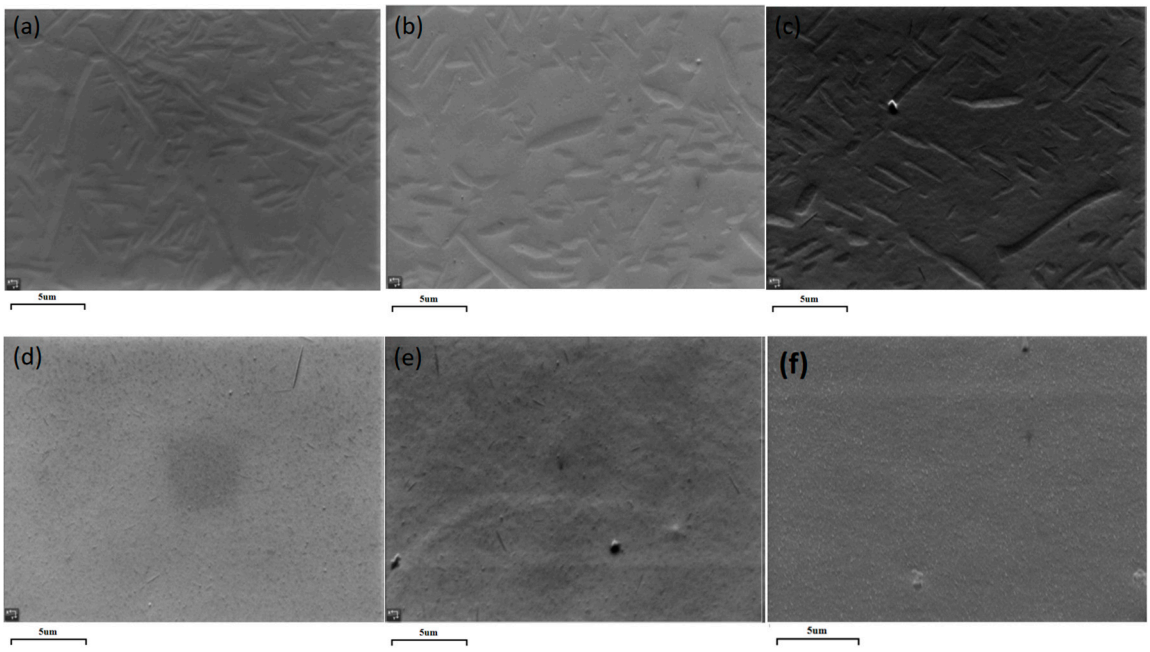


Figure 13. SEM photograph of alloy after experiment. Before annealing: (**a**) 850 °C, 0.01 s^{-1}; (**b**) 850 °C, 1 s^{-1}; (**c**) 910 °C. After annealing: (**d**) 850 °C, 0.01 s^{-1}; (**e**) 850 °C, 1 s^{-1}; (**f**) 910 °C, 1 s^{-1}.

The EBSD maps of Ti-55531 alloy are shown in Figure 14. The inverse pole figures (IPFs) map and recrystallization map are on the left and right side of Figure 14, respectively. The deformation microstructures are divided into dynamic recrystallization grains, sub-grains, and deformed grains according to the grain orientation spread values, marked with blue, yellow, and red in the recrystallization map, respectively [21]. At a temperature of 850 °C, the dynamic recrystallization (DRX) volume fraction increased from 38.5% at 0.01 s^{-1} to 51.4% at 1 s^{-1}, as seen in Figure 14(b1,c1). The dynamic recrystallization volume fraction went from 51.4% at 850 °C to 63.3% at 950 °C at strain rate 1, as seen in Figure 14(c1,d1). After recrystallisation annealing (heating temperature 750 °C, holding time 3 h, air-cooling), the recrystallisation volume fraction of compressed samples under different conditions increased sharply. At a temperature of 850 °C, the dynamic recrystallization (DRX) volume fraction increased from 38.5% at 0.01 s^{-1} to 72.6% at 0.01 s^{-1}, as seen in Figure 14(b1,e1). At the temperature of 850 °C, the dynamic recrystallization (DRX) volume fraction increased from 51.4% at 1 s^{-1} to 76.6% at 1 s^{-1}, as seen in Figure 14(c1,f1). At the temperature of 910 °C, the dynamic recrystallization (DRX) volume fraction increased from 63.3% at 0.01 s^{-1} to 91.2% at 1 s^{-1}, as seen in Figure 14(d1,g1). This was because as the heating temperature increases, recrystallization of the metal occurs and the original grains are replaced by new, defect-free grains, and the degree of recrystallization increases. The influence of temperature on dynamic recrystallization is more complex. This is because a lower temperature is not conducive to the dislocation slippage and climbing of the material, allowing sufficient dislocation entanglement to develop inside the grain. In addition, the presence of more α phase at low temperatures impedes dislocation movement, which promotes nucleation of recrystallized grains [22]. It is worth noting that although a higher

deformation temperature is not conducive to the nucleation of recrystallized grains, this will lead to a much higher growth rate of recrystallized grains [23,24].

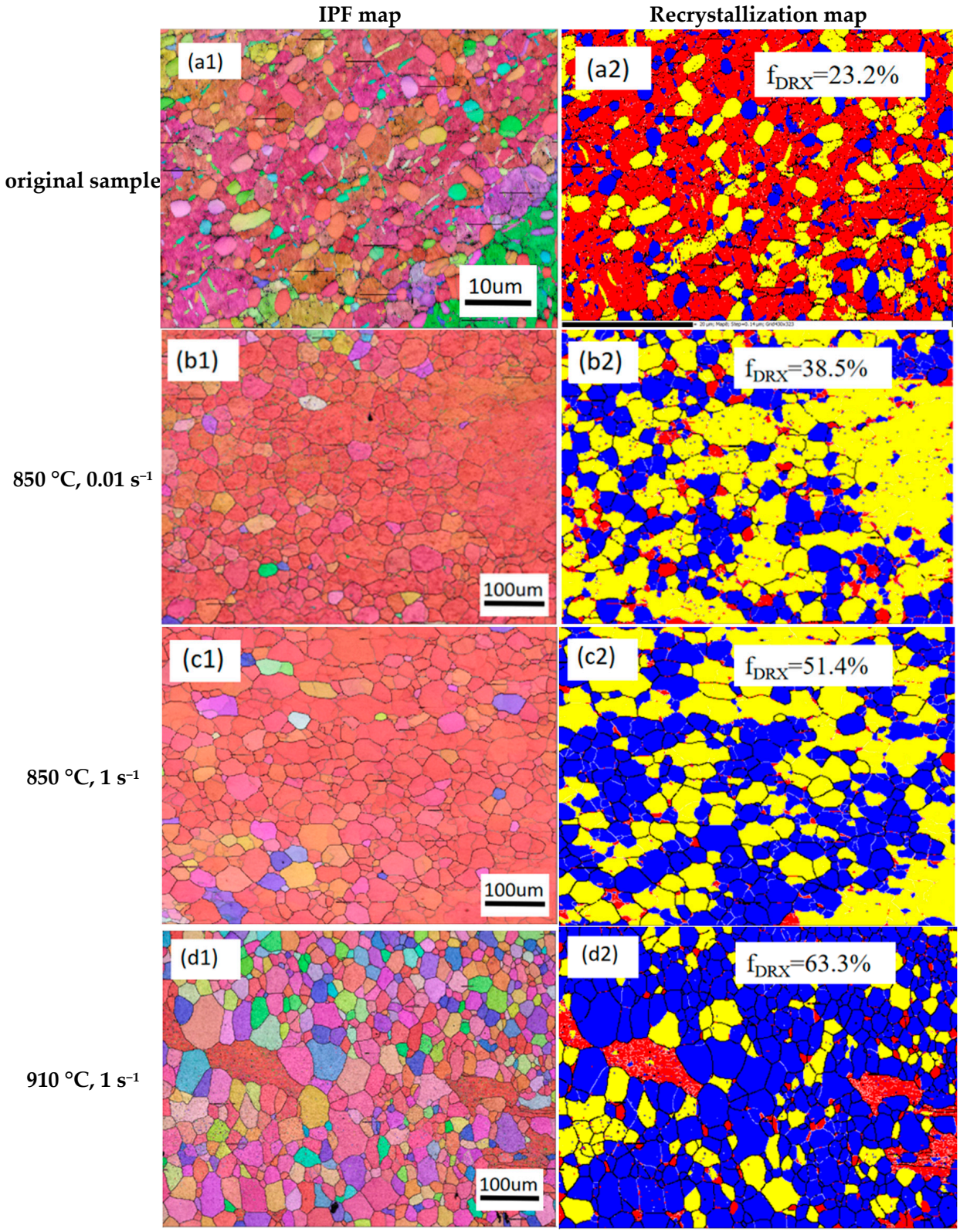


Figure 14. *Cont.*

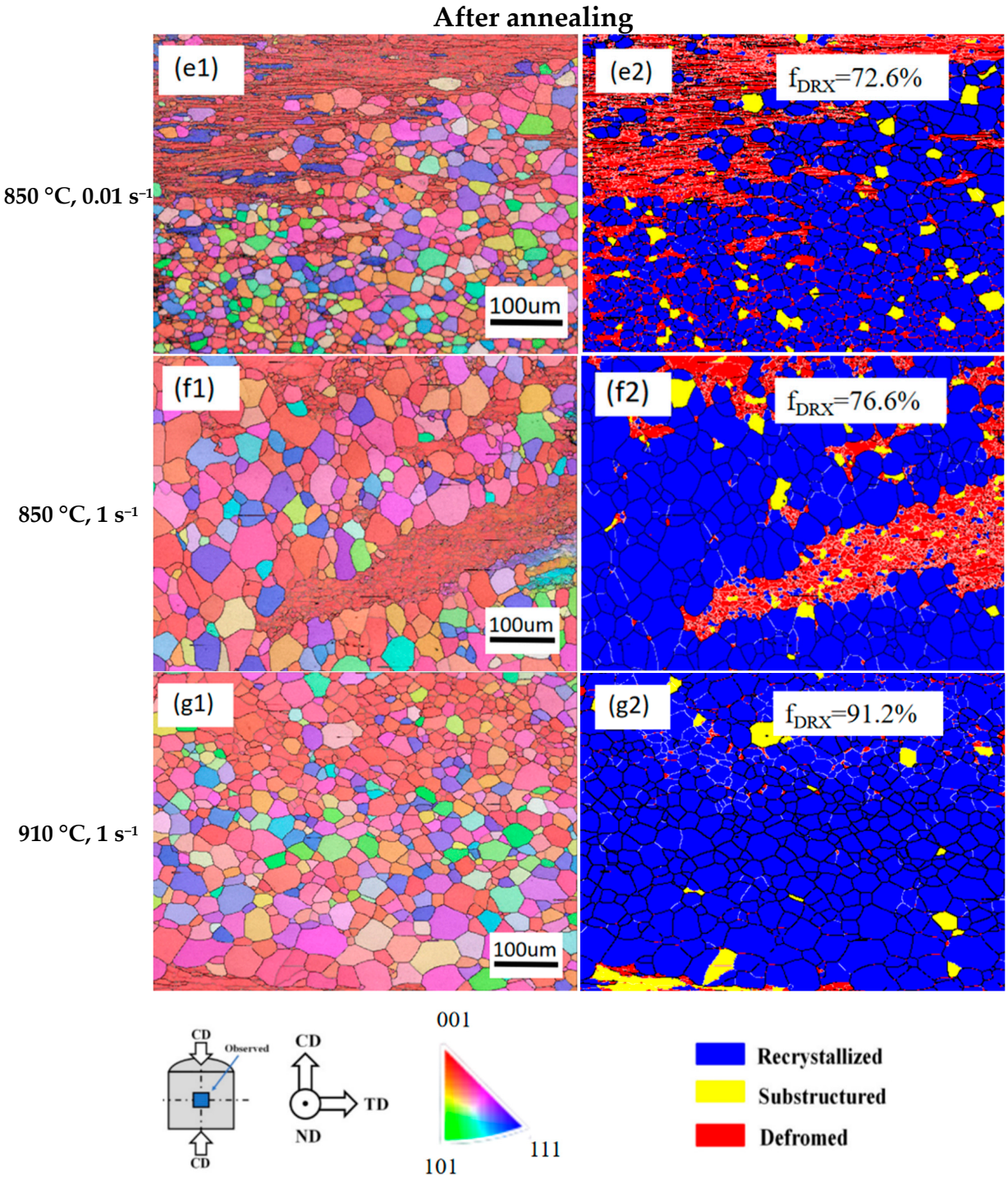


Figure 14. EBSD diagrams of Ti-55531 alloy at various deformed conditions: (**a1**–**g1**): IPF map. (**a2**–**g2**): Recrystallization map.

Following the hot compression process, titanium alloy will produce a large number of internal dislocations and other defects; the accumulation of these defects to a certain extent will trigger dynamic recrystallisation, resulting in new equiaxed grains in the deformation of the organization of the nucleation and growth, to replace the original deformation of the grain. The titanium alloy has a normal grain growth phenomenon. In a high-temperature environment, the atomic diffusion rate is accelerated, the boundary between grains is migrated, and small grains are gradually annexed by large grains, resulting in a larger grain size.

4. Conclusions

The deformation behavior and DRX of Ti55531 titanium alloy were investigated by means of thermal compression tests and metallographic analysis. Based on the experimental results, an ontological model of thermal deformation was developed and the microstructure evolution was analyzed by means of a recrystallization annealing heat treatment process. Several important conclusions can be drawn from the experimental results.

1. The Arrhenius-type ontological equation of Ti55531 titanium alloy was established: $\varepsilon = 2.46 \times 10^7 [sinh(0.0114\sigma)]^{2.8735} exp\left(\frac{-211747.5}{RT}\right)$. The heat deformation activation energy of Ti55531 titanium alloy was obtained to be 211,747.5 kJ·mol^{-1}.
2. A processing diagram of Ti55531 alloy was established, and the alloy has no destabilization zone under the considered test conditions (temperature of 790–940 °C, deformation rate of 0.01–1 s^{-1}). That is, the thermal deformation conditions are all in the thermal deformation safety zone, and flow instability increases with an increase in strain.
3. The EBSD results show that the recrystallized volume fraction increased considerably after hot pressing, with the recrystallized volume fraction of the original samples being 23.2%, which increased to 38.5% at a deformation temperature of 850 degree Celsius and a deformation rate of 0.01, and further increased to 72.6% after annealing treatment. At a deformation temperature of 850 degrees Celsius and a deformation rate of one, the recrystallized volume fraction increased to 51.4%, and after annealing, the recrystallized volume fraction further increased to 76.6%. At a deformation temperature of 910 degrees Celsius and a deformation rate of one, the recrystallized volume fraction increased to 63.3%, and after annealing, the recrystallized volume fraction further increased to 91.2%. These data show that the higher the deformation temperature and deformation rate in the hot pressing process, the higher the recrystallisation volume fraction. After annealing, the recrystallisation volume fraction further increases.

Author Contributions: Conceptualization: Y.Y. (Yucheng Yang) and Z.L.; methodology, Y.Y. (Yucheng Yang) and Y.Y. (Yupeng Yuan); software, Y.Y. (Yucheng Yang) and W.C.; validation, Y.Y. (Yucheng Yang), T.D. and H.L.; formal analysis, H.L.; investigation, Y.Y. (Yupeng Yuan); resources, W.C.; writing—original draft preparation, Y.Y. (Yucheng Yang); writing—review and editing, T.D.; visualization, Z.L.; supervision, Y.Y. (Yucheng Yang); project administration, Y.Y. (Yucheng Yang); funding acquisition, T.D. All authors have read and agreed to the published version of the manuscript.

Funding: The authors acknowledge the financial support provided by the Jiangxi Provincial Natural Science Foundation (No. 20224BAB204043), Jiangxi Provincial Key Laboratory of High-Performance Steel and Iron Alloy Materials (No. 2024SSY05041), and Jiangxi Provincial Key Laboratory of Power Batteries & Energy Storage Materials (No. 2024SSY10011), and the APC was funded by Yucheng Yang.

Data Availability Statement: The original contributions presented in the study are included in the article, further inquiries can be directed to the corresponding author.

Conflicts of Interest: The authors declare no conflict of interest.

References

1. Tan, K.; Li, J.; Guan, Z.J.; Yang, J.B.; Shu, J.X. The identification of dynamic recrystallization and constitutive modeling during hot deformation of Ti55511 tita-nium alloy. *Mater. Des.* **2015**, *84*, 204–211. [CrossRef]
2. Dikovits, M.; Poletti, C.; Warchnmicka, F. Deformation mechanisms in the near-βtitanium alloy Ti-55531. *Metall. Mater. Trans. A* **2014**, *45*, 1586–1596. [CrossRef]
3. Kar, S.K.; Ghosh, A.; Fulzele, N.; Bhattacharjee, A. Quantitative microstructural characterization of a near beta Ti alloy Ti-5553 under different processing conditions. *Mater. Char.* **2013**, *81*, 37–48. [CrossRef]

4. Wen, D.X.; Lin, Y.C. A new dynamic recrystallization kinetics model for a Nb containing Ni-Fe-Cr-base superalloy considering in fluences of initial δ phase. *Vacuum* **2017**, *141*, 316–327. [CrossRef]
5. Shi, S.X.; Ge, J.Y.; Lin, Y.C.; Zhang, X.Y.; Zhou, K.C. High-temperature deformation behavior and recrystallization mechanism of a near beta titanium alloy Ti-55511 in β phase region. *Mater. Sci. Eng. A* **2022**, *847*, 143335. [CrossRef]
6. Matsumoto, H.; Kitamura, M.; Li, Y.P.; Koizumi, Y. Hot forging characteristic of Ti-5Al-5V-5Mo-3Cr alloy with single metastable β microstructure. *Mater. Sci. Eng. A* **2014**, *611*, 337–344. [CrossRef]
7. Jones, N.G.; Jackson, M. On mechanism of flow softening in Ti-5Al-5Mo-5V-3Cr. *Mater. Sci. Technol.* **2011**, *27*, 1025–1032. [CrossRef]
8. Lu, T.; Dan, Z.H.; Li, T.J.; Dai, G.Q.; Sun, Y.Y. Flow softening and microstructural evolution of near β titanium alloy Ti-35421 during hot compression deformation in the α+β region. *J. Mater. Res. Technol.* **2022**, *19*, 2257–2274. [CrossRef]
9. Warchomicka, F.; Poletti, C.; Stockinger, M. Study of the hot deformation behavior in Ti-5Al-5Mo-5V-3Cr-1Zr. *Mater. Sci. Eng. A* **2011**, *528*, 8277–8285. [CrossRef]
10. Fan, X.G.; Zhang, Y.; Gao, P.F.; Lei, Z.N.; Zhan, M. Deformation behavior and microstructure evolution during hot working of a coarse-grained Ti-5Al-5Mo-5V-3Cr-1Zr titanium alloy in beta phase field. *Mater. Sci. Eng. A* **2017**, *694*, 24–32. [CrossRef]
11. Wu, C.; Huang, L. Hot deformation and dynamic recrystallization of a near-beta titanium alloy in the β single phase region. *Vacuum* **2018**, *156*, 384–401.
12. Liu, Z.; Deng, T.; Ai, R.; Yang, Y.; Yuan, Y.; Chen, W.; He, W.; Li, W.; Xiao, W. Microstructure and properties of Ti55531 alloy subjected to deep cryogenic treatment. *J. Mater. Res. Technol.* **2024**, *31*, 3891–3900. [CrossRef]
13. Zhang, D.; Dong, X.; Xu, Y.; Lu, S.; Wei, K.; Huang, L. Dynamic recrystallization mechanism of Ti-6554 alloy during high-temperature deformation. *J. Alloys Compd.* **2023**, *959*, 170534. [CrossRef]
14. Wang, X.; Zhang, H.; Yuan, T. The constitutive equation of TB3 titanium alloy bar was used for aerospace fasteners. *Mater. Charact.* **2024**, *8*, 21–29. [CrossRef]
15. Zhu, N.; Chen, Q.; Chen, S.; Zuo, S. High-temperature constitutive modelling of dynamic restitution and dynamic recrystallisation of TC11 titanium alloy. *Nonferrous Met. Sci. Eng.* **2024**, *15*, 58–66.
16. Jia, B.; Liu, X.; Gu, Y.; Li, G. Deformation behaviour and intrinsic modelling of Ti-1100 cast alloy. *Rare Met.* **2020**, *42*, 1018.
17. Sellars, C.M.; Mctegart, W.J. On the mechanism of hot deformation. *Acta Metall.* **1966**, *14*, 1136–1138. [CrossRef]
18. Deng, T.; Li, S.; Liang, Y.; Sun, L.; Zhang, H. Material Characterization and Validation for Stress Relaxation of Ti-4Al-1.5Mn Alloy at High Temperature. *Rare Met. Mater. Eng.* **2021**, *50*, 829–834.
19. Xiang, Y.; Xiang, W.; Yuan, W. Flow softening and microstructural evolution of near β titanium alloy Ti-55531 during hot compression deformation in the α+β region. *J. Alloys Compd.* **2023**, *955*, 170165. [CrossRef]
20. Zhang, Q.; Yang, S.; Liu, S.; Zhang, Y.; Chen, L.; Jing, M.; Guo, B. Aging treatment on the microstructure evolution of Ti55531 titanium alloy and the influence of mechanical properties. *Rare Met. Mater. Eng.* **2022**, *51*, 2645–2653.
21. Wright, S.I.; Nowell, M.M.; Field, D.P. A review of strain analysis using electron backscatter diffraction. *Microsc. Microanal.* **2011**, *17*, 316–329. [CrossRef] [PubMed]
22. Liang, H.Q.; Nan, Y.; Ning, Y.Q.; Li, H.; Zhang, J.L.; Shi, Z.F.; Guo, H.Z. Correlation between strain-rate sensitivity and dynamic softening behavior during hot processing. *J. Alloys Compd.* **2015**, *632*, 478–485. [CrossRef]
23. Duan, Y.H.; Ma, L.S.; Qi, H.R.; Li, R.Y.; Li, P. Developed constitutive models, processing maps and microstructural evolution of Pb-Mg-10Al-0.5B alloy. *Mater. Charact.* **2017**, *129*, 353–366. [CrossRef]
24. Zang, Q.H.; Yu, H.S.; Lee, Y.S.; Kim, M.S.; Kim, H.W. Effects of initial microstructure on hot deformation behavior of Al-7.9Zn-2.7Mg-2.0Cu (wt%) alloy. *Mater. Charact.* **2019**, *151*, 404–413. [CrossRef]

Disclaimer/Publisher's Note: The statements, opinions and data contained in all publications are solely those of the individual author(s) and contributor(s) and not of MDPI and/or the editor(s). MDPI and/or the editor(s) disclaim responsibility for any injury to people or property resulting from any ideas, methods, instructions or products referred to in the content.